Zhang *et al. Chem Synth* 2024;4:79
DOI: 10.20517/cs.2024.116

Chemical Synthesis

Research Article

Open Access

A new approach for methane oxidation: photocatalytic ozonation over noble metal decorated zinc oxide nanocatalysts

Haiyuan Zhang[1], Yun Wang[1], Jiahua Zhu[1], Xiaohua Lu[1], Yang Bai[2], Wei Li[2,*], Liwen Mu[1,*]

[1]State Key Laboratory of Materials-oriented Chemical Engineering College of Chemical Engineering, Nanjing Tech University, Nanjing 211816, Jiangsu, China.
[2]Institute for Materials and Processes School of Engineering, The University of Edinburgh, Edinburgh EH9 3FB, Scotland, UK.

[*]**Correspondence to:** Prof. Liwen Mu, State Key Laboratory of Materials-oriented Chemical Engineering College of Chemical Engineering, Nanjing Tech University, 30 South Puzhu Road, Nanjing 211816, Jiangsu, China. E-mail: lwmu@njtech.edu.cn; Prof. Wei Li, Institute for Materials and Processes, School of Engineering, The University of Edinburgh, Robert Stevenson Road, Edinburgh EH9 3FB, Scotland, UK. E-mail: wei.li@ed.ac.uk

How to cite this article: Zhang H, Wang Y, Zhu J, Lu X, Bai Y, Li W, Mu L. A new approach for methane oxidation: photocatalytic ozonation over noble metal decorated zinc oxide nanocatalysts. *Chem Synth* 2024;4:79. https://dx.doi.org/10.20517/cs.2024.116

Received: 30 Aug 2024 **First Decision:** 31 Oct 2024 **Revised:** 20 Nov 2024 **Accepted:** 29 Nov 2024 **Published:** 12 Dec 2024

Academic Editor: Ying Wan **Copy Editor:** Pei-Yun Wang **Production Editor:** Pei-Yun Wang

Abstract

We designed a new approach to oxidize methane, a potent greenhouse gas. In this approach, the synergistic effect of photocatalytic ozonation is utilized to oxidize methane at low concentrations. Using ZnO nanomaterials modified with noble metals (i.e., Au, Pt, and Pd), results show that the catalytic oxidation of methane is generally significantly improved by the synergistic system approach. More specifically, the efficiency of photocatalytic ozonation was at least two times higher than the sum of the contributions from individual sub-processes (i.e., photocatalysis, catalytic ozonation, and ozone photolysis), and the synergistic effect was effectively utilized. The durability of the catalysts is another highlight, with no decrease in activity over ten cycles. Based on the experimental results, combined with the characterization, and taking Au/ZnO as an example, it can be seen that Au/ZnO with high specific surface area and high adsorption capacity is more conducive to ozone adsorption and activation, enhances the formation of active radicals ($\cdot O_2^-$ and $^1O_2$) and promotes the synergistic effect. Meanwhile, we believe that the larger Au nanoclusters and the zero-valent stabilized Au are important reasons for the durability of the catalyst. This work provides a novel approach to removing low-concentration methane and guides further development of a practical photocatalytic ozonation system.

Keywords: Methane oxidation, photocatalytic ozonation, synergistic effect

INTRODUCTION

Methane, the primary component of natural gas, is widely used as a fuel, but it is also a potent greenhouse gas second only to carbon dioxide. A molecule of methane will cause 28-36 times the greenhouse effect of that of carbon dioxide over a 100-year period[1,2]. Methane has a short life cycle in the atmosphere (about 12 years), and atmospheric methane concentration can respond to methane removal relatively quickly, which is the most direct and effective way to slow down the rate of climate warming in the short term[3,4].

Methane is characterized by inertness (bond energy = 434 $kJ \cdot mol^{-1}$), and fugitive methane emissions are usually in low concentration (most methane emission concentrations are below 2,500 ppm)[4,5]. Efforts of developing effective approaches to remove methane have to tackle these two challenges.

Recent research explored photocatalytic reactions, which can oxidize methane at mild reaction conditions and with minimum energy input[2,6,7], such as CuO/ZnO[7] and Ag/ZnO[8] for photocatalytic oxidation of methane at 100 ppm[9-11]. At the same time, researchers are actively looking for other approaches, such as biological methane removal (including biotrickling filters[12]), managing soils in agricultural or other ecosystems (soil amendments[13]), and iron-salt aerosol formation[14,15].

The combination of ozone and photocatalysis (photocatalytic ozonation) is also a promising advanced oxidation technology, as it has shown potential for the degradation of a wide range of pollutants[16-18]. In theory, when the photocatalysis and ozone oxidation are carried out at the same time, ozone is capable of absorbing ultraviolet (UV) light below 310 nm, photolyzes, and forming reactive oxygen species[19]. Simultaneously, photocatalysts produce photogenerated carriers on the surface to initialize the redox reactions. During the process, electrophilic ozone chemisorbs on the catalyst surface by inserting an O atom into an oxygen vacancy and acts as an electron donor[20,21]. It can prevent the recombination of charge carriers and increase the number of photogenerated carriers involved in the reaction. In addition, due to the transfer of excess electrons near the oxygen vacancy to the O atom of ozone, charged oxygen species (such as O_2^-, $^1O_2$) are formed, accelerating ozone decomposition[22,23]. At the same time, the adsorption equilibrium of the reactant at the adsorption site, the migration of the reactant to the surface active site, and the reaction between the reactant and the active substances all work together to enhance the oxidation process. This synergistic effect of photocatalytic ozonation retains the high mineralization degree of photocatalytic oxidation and the high efficiency of ozone oxidation, solving the bottlenecks of high photocatalytic carrier recombination rate and incomplete ozone mineralization[6,16,24].

In reality, efforts have been made to apply photocatalytic ozonation to various gaseous[18,25,26] and aqueous[27-29] matrices, achieving excellent pollutant oxidation rates in some cases. However, two issues still need to be addressed: (i) In numerous instances, the actual efficiency is unsatisfactory because the photocatalyst cannot effectively activate ozone[24,30]; (ii) How to maintain the stability of the photocatalyst in the reaction because of the strong oxidation of ozone[6,16].

Due to the following advantages of the noble metal modification: (i) The modification of noble metal nanoparticles can effectively store electrons and thus activate ozone; (ii) Noble metals are not easily oxidized or reduced in chemical reactions and can maintain high activity in multiple reaction cycles[31-35]. In this paper, we employed the noble metals Au, Pt, and Pd to modify semiconducting ZnO to investigate the application of photocatalytic ozonation in low-concentration methane oxidation and demonstrated the excellent efficiency and durability of the method. Among them, the Au/ZnO catalysts: (i) High specific surface area and adsorption capacity are more conducive to ozone adsorption and activation, enhancing the generation of active radicals ($\cdot O_2^-$, $^1O_2$) and promoting synergistic effects; (ii) Larger gold nanoclusters and

zero-valent stabilized gold enable the catalysts to maintain good durability in cyclic reactions.

EXPERIMENTAL

Materials

Zinc nitrate hexahydrate [$Zn(NO_3)_2·6H_2O$], oxalic acid dihydrate ($H_2C_2O_4·2H_2O$), sulfuric acid (H_2SO_4) and sodium borohydride ($NaBH_4$) were provided by Shanghai Lingfeng Chemical Reagent Co., LTD. Palladium nitrate dihydrate [Pd $(NO_3)_2·2H_2O$] was provided by Jiuding Chemical (Shanghai) Technology Co., LTD. Tetrachloro-gold hydrate ($HAuCl_4·4H_2O$) was provided by Tianjin Xiensi Biochemical Technology Co., LTD. Chloroplatinic acid hexahydrate ($H_2PtCl_6·6H_2O$), ferric oxide (Fe_2O_3), manganese dioxide (MnO_2) and sodium thiosulfate ($Na_2S_2O_3·5H_2O$) were provided by Shanghai McLean Biochemical Technology Co., LTD. Soluble starch [$(C_6H_{10}O_5)_n$] was provided by Shanghai Sinopharm Chemical Reagent Co., LTD. Potassium iodide (KI) was provided by Shanghai Aladdin Biochemical Technology Co., LTD. All of these chemicals were used as received without further purification.

Sample preparation

Zinc oxide (ZnO) nanoparticles were synthesized by precipitation method. Initially, 14.87 g of zinc nitrate [$Zn(NO_3)_2·6H_2O$, 0.05 mol] and 6.3 g of oxalic acid ($H_2C_2O_4·2H_2O$, 0.05 mol) were weighed and dissolved in 1 L of deionized water, respectively. Subsequently, the $H_2C_2O_4$ solution was added dropwise as a precipitating agent to obtain the white precipitate of zinc oxalate (ZnC_2O_4). The precipitate was centrifuged, washed, and dried at 60 °C for 2 h. Then, the ZnC_2O_4 precipitate was calcined at 350 °C for 6 h to yield ZnO.

To synthesize the ZnO compound supported by 0.1 wt% noble metal, 1 g ZnO was dispersed into 100 mL deionized water using ultrasonic waves, and a metal precursor with a mass fraction of 0.1 wt% was added. For example, to prepare 0.1 wt% Au/ZnO, 1.82 mg $HAuCl_4·4H_2O$ was required. After stirring for 30 min, a quantity of freshly prepared $NaBH_4$ aqueous solution was dropped into the solution. It was stirred again for 2 h, centrifuged for collection, washed, and dried at 60 °C. The synthesis of 0.1 wt% Pt, Pd/ZnO catalysts followed a similar procedure, with the only variation being the use of the corresponding metal precursor.

To synthesize the ZnO compound supported by 0.1 wt% non-noble metal, 1 g ZnO was dispersed into 100 mL deionized water using ultrasonic waves, followed by adding a metal precursor with a mass fraction of 0.1 wt%. For instance, to prepare 0.1 wt% Mn/ZnO, 1.58 mg MnO_2 was needed. The mixture was stirred again for 2 h, centrifuged for collection, washed, and dried at 60 °C. The synthesis of 0.1 wt% Fe/ZnO catalysts followed a similar procedure, with the only difference being the choice of the metal precursor.

Characterization

Powder X-ray diffraction (PXRD) characterized the crystal structures of the obtained samples on a Bruker/AXS D8 Advance diffractometer using Cu Kα radiation and a nickel filter (λ = 0.15406 nm). The microstructure was imaged by scanning electron microscopy [field emission scanning electron microscopy (FESEM), TESCAN Mira4] and high-resolution transmission electron microscopy (HR-TEM, JEOL JEM-2100Plus, Japan). The valence states and doping amounts of the samples were studied by X-ray photoelectron spectroscopy (XPS, Thermo Fischer, ESCALAB Xi+) using Al-Ka radiation (1,486.6 eV). The binding energy of C1s (284.8 eV) was used for calibration. A UV-visible (Vis)-near-infrared spectrophotometer (METASH, X-3) was used to collect UV-Vis absorption spectra. $BaSO_4$ was used as the reflectivity standard, and the XPS-valence band (VB) spectrum was used to estimate the VB position of ZnO. The Brunauer–Emmett–Teller (BET) surface area of the samples was determined by a TriStarII3020 surface area analyzer. For Raman backscattering spectroscopy measurements, the sample is excited by a 514 nm laser beam with a scanning range of 100-1,000 cm^{-1}, and the scattered Raman signal is recorded with a LabRam HR800 confocal microraman spectrometer.

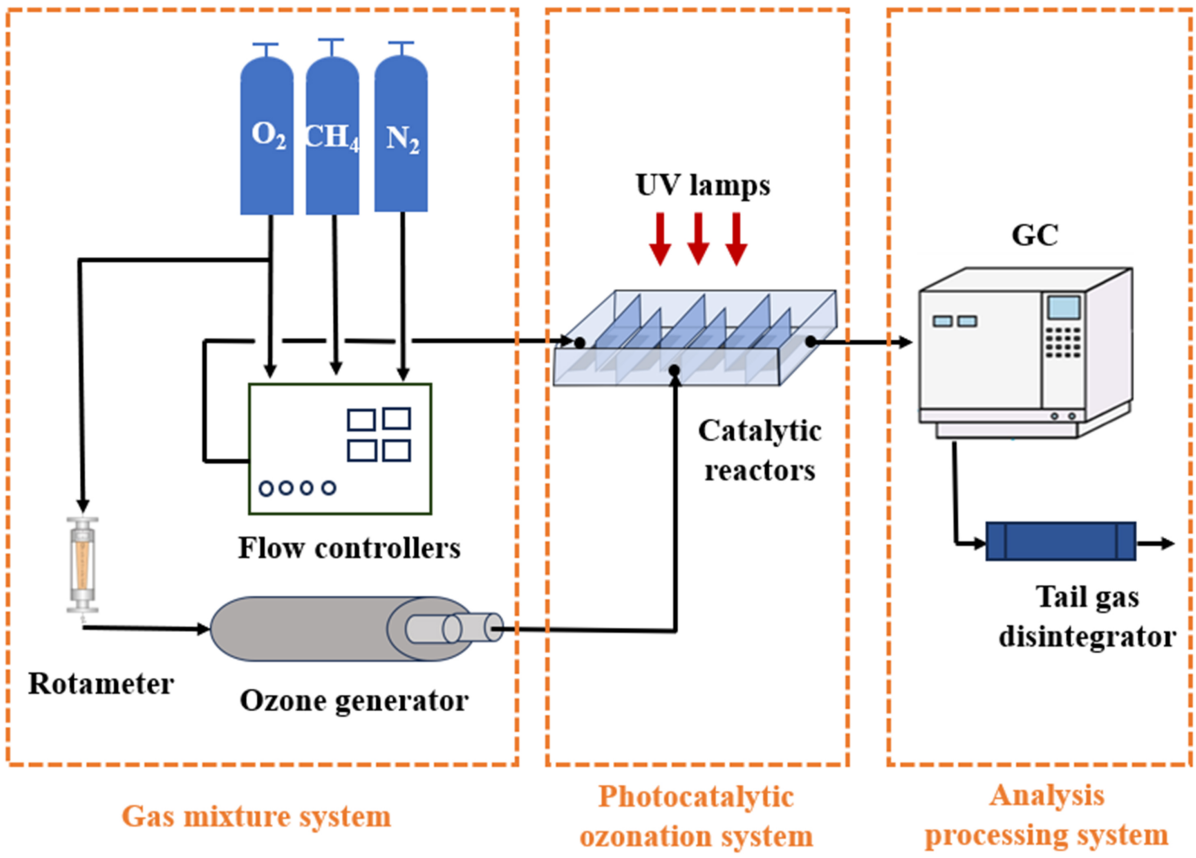

Figure 1. Diagram of the photocatalytic ozonation reaction system.

Photocatalytic ozonation to methane conversion experiment

In the typical photocatalytic ozonation of methane, a continuous flow reactor with a volume of 450 mL was used to perform methane photocatalytic ozonation experiments at room temperature [Figure 1]. Baffles were incorporated within the reactor to extend the gas retention time. Additionally, 0.5 g photocatalyst is filled into the reactor, and the carbon dioxide and water adsorbed on the catalyst and reactor are removed with flowing N_2. The total flow rate is 200 mL·min^{-1}, which contains 25 mL·min^{-1} 140 ppm methane, 75 mL·min^{-1} nitrogen and 100 mL·min^{-1} ozone of a certain concentration (0, 75, 150, 300 ppm). Two 14 W 254 nm UV lamps (GHP287T5L/4) with an intensity of ~8 mW·cm^{-2} were utilized to provide light for the catalytic reaction. Intermediate analysis was carried out by gas chromatograph (GC7920GTF2ZV). Calibration curves were plotted using the external reference method [Supplementary Figures 1-3] to determine the concentrations of both reactants and products. The gas chromatography outlet gas was collected before and after 5 and 30 min of reaction to analyze the ozone concentration data by iodometric method[36]. Specific details can be found in the Supplementary Materials (as shown in "Iodometric determination of ozone concentration"). In addition, an exhaust gas decomposer was installed at the end of the detection system to decompose any unreacted ozone.

RESULTS AND DISCUSSION

Performance evaluation

The photocatalytic ozonation reaction device is shown in Figure 1. Compared with other research teams, we reduced the amount of catalyst per unit area and the required light intensity[7,8], and used ozone instead of oxygen as an oxidant; the advantages can be summarized as follows: (i) Higher electron affinity (EA) than

O_2 (2.10 *vs.* -0.33 eV), trapping electrons to reduce carriers recombination[24]; (ii) The wavelength < 310 nm (such as the 254 nm UV used in the experiment) promotes the photodissociation of ozone, generates reactive oxygen species and further improves the oxidation capacity of the system[19]; (iii) In photocatalytic ozonation, methane oxidation expands from heterogeneous systems (e.g., photocatalytic and catalytic ozonation) to homogeneous systems (e.g., ozone photolysis). The synergistic effect between the catalyst, ozone and UV makes the photocatalytic ozonation efficiency higher than the sum of the efficiencies of the individual oxidation processes[6].

Figure 2A and Supplementary Figure 4 show the methane conversion rates of noble and non-precious metal-modified ZnO under different oxidation processes. The experimental results confirm the above observation that the contribution of the mixed oxidation process is greater than the sum of the contributions of the individual sub-processes. In particular, the efficiency of Au/ZnO photocatalytic ozonation (56.12%) was at least two times higher than the sum of the contributions from individual sub-processes and four times higher than photocatalysis alone (13.92%) [Figure 2B]. Compared with the oxidation products of photocatalytic and photocatalytic ozone oxidation [Supplementary Figure 5], photocatalytic methane oxidation can be completely converted to CO_2. It exhibits low conversion rate but high mineralization rate. Photocatalytic ozonation produces a very small amount of CO as a by-product, but still has a large performance advantage in the overall comparison.

We also tested the performance of the Au/ZnO material at different ozone concentrations. The mineralization rate and reaction rate of methane oxidation increased with ozone concentration [Figure 2C], further confirming the advantages of ozone introduction. After ten photocatalytic ozone cycles [Figure 2D, Supplementary Figure 6], the Au, Pt-modified ZnO maintained its original activity without significantly decreasing. However, Pd/ZnO shows a slight decrease (37.26%-34.91%) in performance after the introduction of ozone.

In addition, to study ozone utilization, we measured the ozone concentration before and after the photocatalytic ozonation. Within five minutes of turning on the UV light, the ozone concentration decreased from ~300 to ~78 ppm [Supplementary Table 1] and did not change for 30 min. There was no significant difference between the different catalysts. Under the same lighting conditions, ozone photolysis produces equal amounts of mono- and dioxygen atoms. The utilization rate of specific catalysts for active oxygen is difficult to quantify at this time and will need to be further investigated at a later stage.

Structure and morphology

In order to observe the structure and microscopic morphology of the catalyst, we conducted the corresponding characterization. In Figure 3A, the PXRD diffraction peaks can be well assigned to hexagonal wurtzite ZnO (JCPDS No. 79-0206)[7]. Due to the low loading and uniform dispersion of precious metals, no corresponding diffraction peaks are observed, indicating that the load of noble metals on ZnO does not alter its crystal structure. Figure 3B shows the Raman spectra of pure ZnO and ZnO composite samples. Two characteristic peaks of the hexagonal wurtzite ZnO are observed at 437 and 330 cm^{-1}, corresponding to the $E_{2(High)}$ and the $E_{2(High)}$ - $E_{2(Low)}$ modes associated with significant vibrations of the Zn sublattice, respectively. The peak at 583 cm^{-1} is assigned to the longitudinal optical component of the E_1 mode[28,29,37]. Comparing the peak positions and intensities of the materials, it is observed that the characteristic peaks are slightly shifted after loading. The intensity of the characteristic spectral bands of ZnO increases marginally following the addition of Au, which can be attributed to the resonance enhancement effect resulting from the localized electric field created by Au on the surface of ZnO. Furthermore, noble metal nanoparticles and mesoporous ZnO exhibit strong metal-support interactions (SMSI), which alter the molecular vibration frequency and

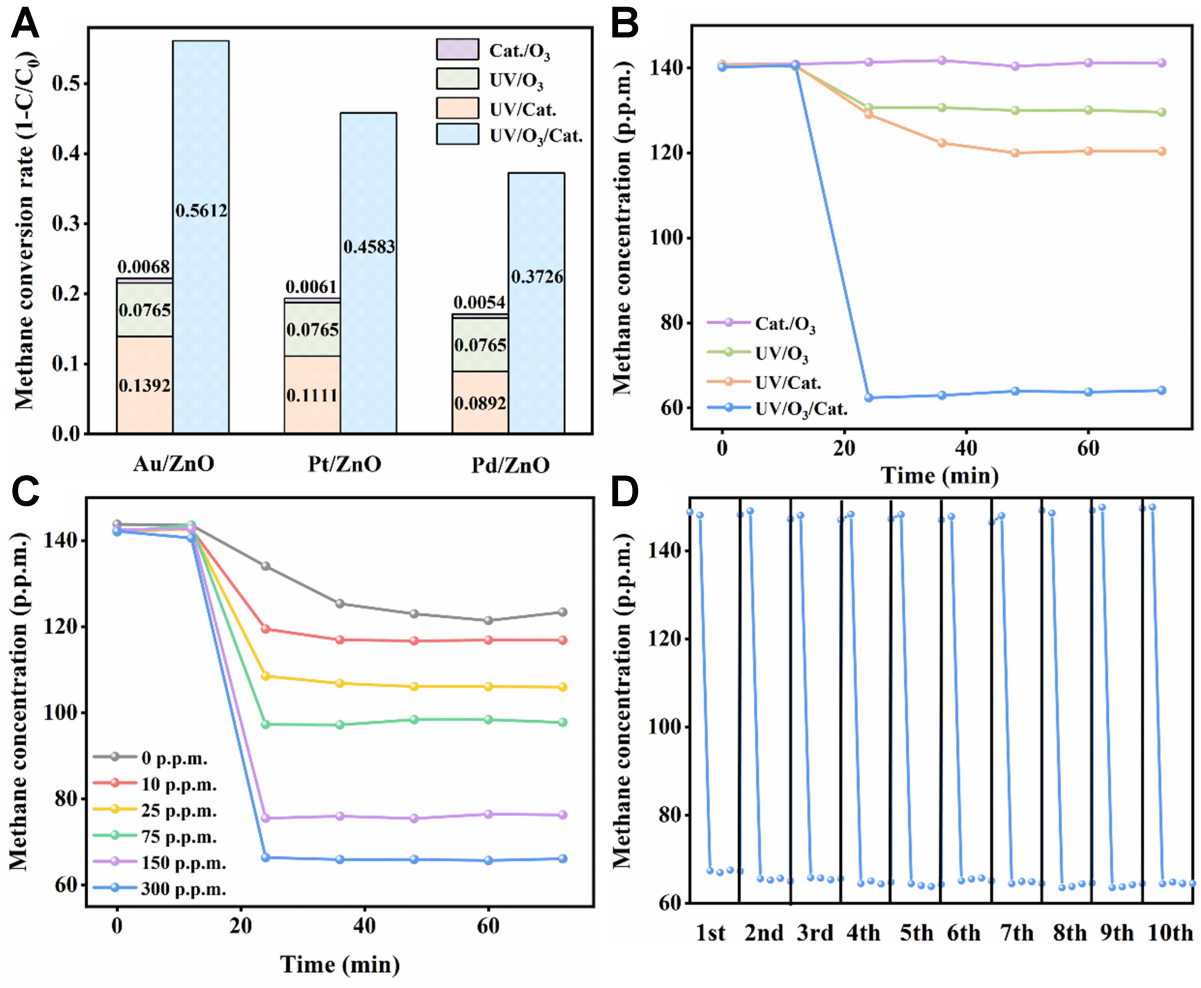

Figure 2. Methane photocatalytic ozonation in continuous flow reactor. (A) Methane conversion of various catalysts under different oxidation processes; (B) Variation of methane concentration under different oxidation processes over the Au/ZnO (Reaction condition: 0.5 g photocatalyst, reaction temperature of 25 ± 2 °C, light intensity: 16 W 254 nm UV*2, gas flow rate: 200 mL·min^{-1}, ozone concentration: 300 ppm); (C) Variation of methane concentration at different ozone concentrations over the Au/ZnO; (D) Cyclic tests of photocatalytic ozonation over the Au/ZnO (One cycle: 4 h; ten cycles: 40 h). UV: Ultraviolet.

contribute to the displacement of the Raman peak[37].

Figure 3C shows that the ZnO powder consists of irregular spheres with an average particle size of approximately 20 nm. HR-TEM images [Figure 3D] clearly illustrate the deposition of Au on the surface of ZnO. Compared to Pt/ZnO and Pd/ZnO materials [Supplementary Figure 7], the modification with Au results in the formation of larger clusters, approximately 5 nm. These clusters are not easily oxidized by ozone, which may account for the stability of the catalyst in cycling experiments.

In addition, the surface area and pore structure of ZnO and its composites were also examined [Supplementary Table 2]. Compared to other samples, the Au/ZnO catalysts exhibited a high specific surface area and adsorption capacity [Supplementary Figure 8], which may expose more active sites. This characteristic is more conducive to ozone adsorption and activation. In general, the metal will partially fill the pores under load; the unusual phenomenon observed with Au loading may be attributed to some interstices and voids created by the stacking of nanoparticles and clusters[38-40].

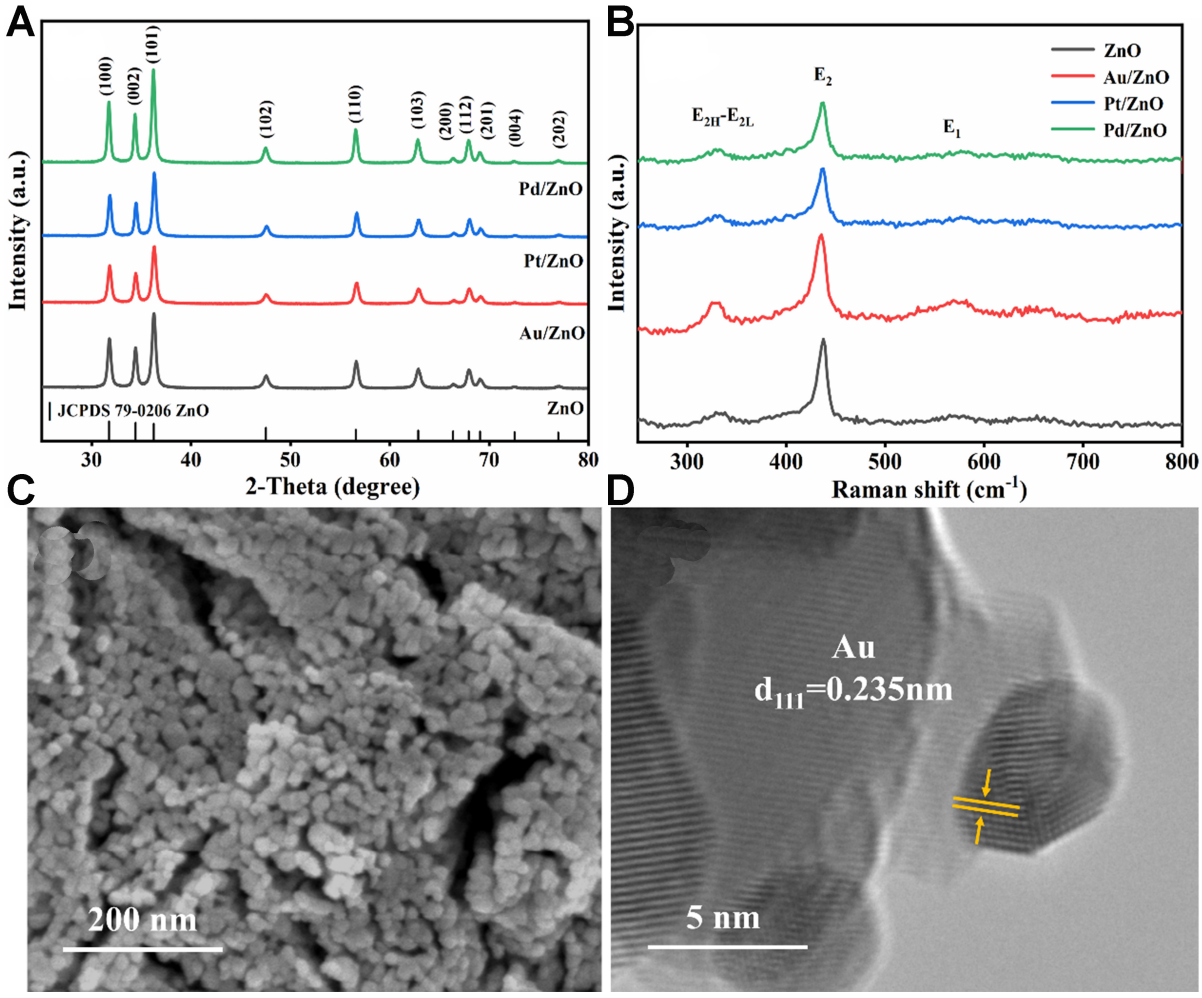

Figure 3. (A) PXRD patterns, (B) Raman spectra of the samples, (C) SEM, (D) HR-TEM images of 0.1 wt% Au/ZnO. PXRD: Powder X-ray diffraction; SEM: scanning electron microscopy; HR-TEM: high-resolution transmission electron microscopy.

Chemical valence

XPS [Figure 4] was utilized to confirm the chemical valence state of Au and to assess its stability following photocatalytic ozonation reactions. Figure 4A shows the survey spectrum of 0.1 wt% Au/ZnO[41]. In Figure 4B, the O 1s spectrum can be fitted to three peaks of 529.9, 531.2 and 532.0 eV, corresponding to lattice oxygen, oxygen vacancy and surface adsorbed oxygen[29,42]. Due to the partial overlap of the Zn 3p and Au 4f orbitals, along with the strong peak intensity of Zn 3p, it is impossible to discern the information of Au at a low loading of 0.1 wt% [Figure 4C]. However, when the Au loading is increased to 0.5 wt% [Figure 4D], the peaks centered at 83.3 and 86.9 eV correspond to Au $4f_{7/2}$ and Au $4f_{5/2}$, respectively, confirming the existence of Au^0[41,43]. Combined with PXRD spectra [Supplementary Figure 9], no changes were observed in the structure and valence state of the Au/ZnO before and after the photocatalytic ozonation reaction.

Supplementary Figure 10 shows that Pt^{2+} does not change its valence state before and after the reaction[44,45], while Pd was oxidized by ozone from its zero valence state to +2[46,47]. This suggests that Pd may have been oxidized during the reaction and could not remain stable. This corresponds to the results of the photocatalytic ozonation cycle [Supplementary Figure 6].

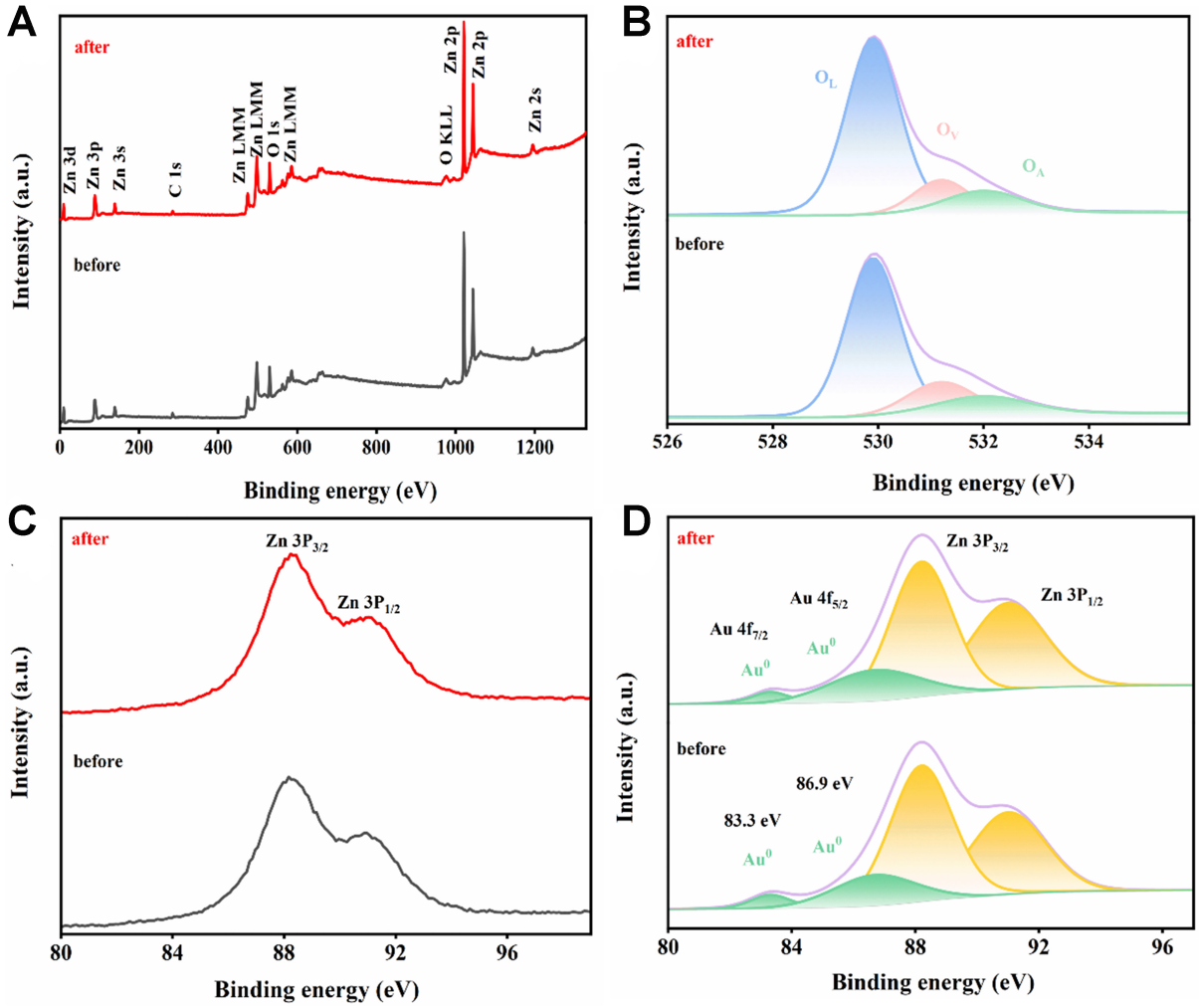

Figure 4. XPS spectrum of Au/ZnO before and after photocatalytic ozonation reactions. (A) Survey spectrum (0.1 wt% Au/ZnO); (B) XPS spectrum of O 1s (0.1 wt% Au/ZnO); (C) XPS peaks for Au $4f_{7/2}$, Au $4f_{5/2}$, Zn $3p_{1/2}$ and Zn $3p_{3/2}$ (0.1 wt% Au/ZnO); (D) XPS peaks for Au $4f_{7/2}$, Au $4f_{5/2}$, Zn $3p_{1/2}$ and Zn $3p_{3/2}$ (0.5 wt% Au/ZnO). XPS: X-ray photoelectron spectroscopy.

Reaction mechanism

UV-Vis diffused reflectance spectra [Supplementary Figure 11A] and XPS-VB spectra [Supplementary Figure 11B] were utilized to determine the band gap of ZnO (Eg = 3.21 eV), Au/ZnO (Eg = 3.19 eV) and the conduction band (CB), VB positions of ZnO. The instrument work function φ is 4.62 eV. Therefore, the VB of ZnO is calculated to be 2.78 eV, and the CB is -0.43 eV ($E_{VB, NHE} = \varphi + E_{VB, XPS} - 4.5$).

Based on the catalyst energy band structure, we proposed a probable mechanism for methane oxidation during photocatalytic ozonation process [Figure 5]. Initially, the catalyst generates photogenerated electrons and holes when exposed to UV light [Equation (1)]. Since the redox potential of $CH_4/\cdot CH_3$ is 0.83 V *vs.* normal hydrogen electrode (NHE), the VB position of ZnO (2.78 V *vs.* NHE) thermodynamically facilitates the conversion of CH_4 to $\cdot CH_3$ under the action of holes [Equation (2)][29]. When strong electrophilic ozone is introduced, in addition to the direct reaction between ozone and methane, the synergistic effect can be explained as: (i) The 254 nm UV wavelength promotes the photodissociation of O_3 to form reactive oxygen ($\cdot O$) [Equation (3)][19]; (ii) The higher EA of O_3 is more conducive to trapping electrons at the CB [Equation (4)] to product $\cdot O_3^-$[22,24]; (iii) $^1O_2$ is most likely to be produced by dissociation of O_3 [Equation (5)] and $\cdot O_2^-$

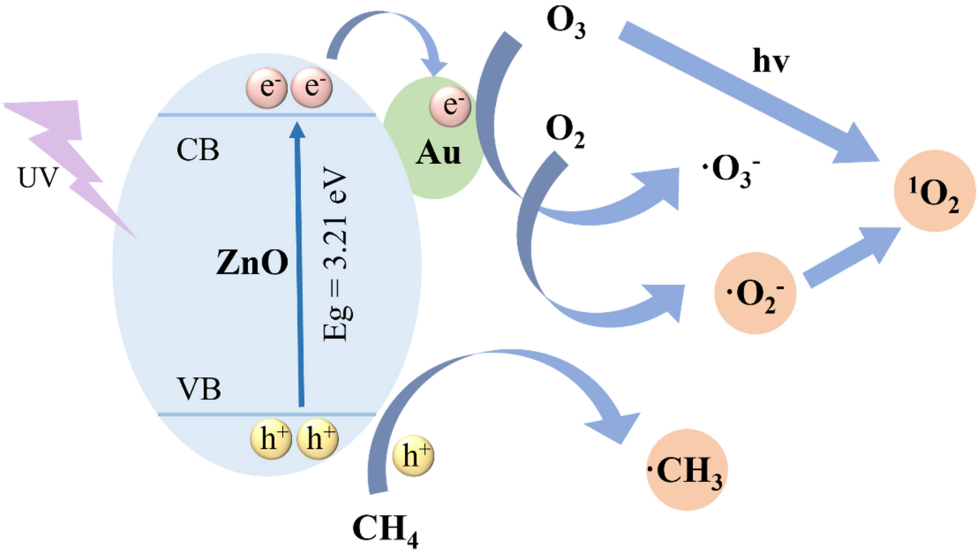

Figure 5. Possible mechanisms for methane removal by photocatalytic ozonation over Au/ZnO.

oxidation by holes [Equation (6)][19,48]. In addition, since E° (O_3/$\cdot O_3^-$) (2.10 V *vs.* NHE) is much higher than E° (O_2/$\cdot O_2^-$) (-0.33 V *vs.* NHE), O_3 can easily pick up electrons from $\cdot O_2^-$ [Equation (7)][23,29].

$$\text{Cat.} + h\nu \rightarrow e^- + h^+ \quad (1)$$

$$CH_4 + h^+ \rightarrow \cdot CH_3 + H^+ \quad (2)$$

$$O_3 + h\nu\ (\lambda < 305\ \text{nm}) \rightarrow {}^1O_2 + \cdot O \quad (3)$$

$$O_3 + e^- \rightarrow \cdot O_3^- \quad (4)$$

$$O_2 + e^- \rightarrow \cdot O_2^- \quad (5)$$

$$\cdot O_2^- + h^+ \rightarrow {}^1O_2 \quad (6)$$

$$O_3 + \cdot O_2^- \rightarrow \cdot O_3^- + O_2 \quad (7)$$

CONCLUSIONS

In conclusion, we have synthesized noble metal-modified ZnO nanocomposites using a simple sodium borohydride reduction method. Based on these photocatalysts, we utilized the synergistic effect between photocatalysis and ozone catalysis to remove low concentrations of methane. The results show that the efficiency of photocatalytic ozonation was at least two times higher than the sum of the contributions from individual sub-processes (i.e., photocatalysis, catalytic ozonation, and ozone) and four times higher than photocatalysis alone. Au-modified ZnO maintains long-term stability after multiple cycles as Au is less affected by ozone oxidation. In addition, the possible mechanism of the synergistic process is discussed. The introduction of ozone promoted the separation of electron holes on the catalyst surface, and more active substances ($\cdot O_2^-$ and $^1O_2$) were generated through the interaction between the catalyst, UV light and ozone to drive the oxidation reaction and promote the synergistic effect.

DECLARATIONS

Authors' contributions

Designed and revised the manuscript: Zhang H, Wang Y, Zhu J, Lu X, Bai Y, Li W, Mu L
Carried out the experiments, tests and analysis: Zhang H, Wang Y

Availability of data and materials

The authors confirm that the data supporting the findings of this study are available within its Supplementary Materials.

Financial support and sponsorship

This research was supported by the National Key Research and Development Plan (Key Special Project of Inter-governmental National Scientific and Technological Innovation Cooperation, Grant No. 2019YFE0197500), the European Commission H2020 Marie S Curie Research and Innovation Staff Exchange (RISE) award (Grant No. 871998), the National Natural Science Foundation of China (Grant Nos. 22178160, 22327809). In addition, Mu L gratefully acknowledges the financial support of the "Jiangsu Specially-Appointed Professor Plan".

Conflicts of interest

All authors declared that there are no conflicts of interest.

Ethical approval and consent to participate

Not applicable.

Consent for publication

Not applicable.

REFERENCES

1. Mozharova NV, Kulachkova SA, Lebed'-Sharlevich YI. Emission and sink of greenhouse gases in soils of Moscow. *Eurasian Soil Sc* 2018;51:359-70. DOI
2. Shah MSA, Oh C, Park H, Hwang YJ, Ma M, Park JH. Catalytic oxidation of methane to oxygenated products: recent advancements and prospects for electrocatalytic and photocatalytic conversion at low temperatures. *Adv Sci* 2020;7:2001946. DOI PubMed PMC
3. Abernethy S, O'Connor FM, Jones CD, Jackson RB. Methane removal and the proportional reductions in surface temperature and ozone. *Philos Trans A Math Phys Eng Sci* 2021;379:20210104. DOI PubMed PMC
4. Hu D, Ordomsky VV, Khodakov AY. Major routes in the photocatalytic methane conversion into chemicals and fuels under mild conditions. *Appl Catal B Environ* 2021;286:119913. DOI
5. Song H, Meng X, Wang Z, Liu H, Ye J. Solar-energy-mediated methane conversion. *Joule* 2019;3:1606-36. DOI
6. Priyadarshini M, Das I, Ghangrekar MM, Blaney L. Advanced oxidation processes: performance, advantages, and scale-up of emerging technologies. *J Environ Manage* 2022;316:115295. DOI PubMed
7. Li Z, Pan X, Yi Z. Photocatalytic oxidation of methane over CuO-decorated ZnO nanocatalysts. *J Mater Chem A* 2019;7:469-75. DOI
8. Chen X, Li Y, Pan X, Cortie D, Huang X, Yi Z. Photocatalytic oxidation of methane over silver decorated zinc oxide nanocatalysts. *Nat Commun* 2016;7:12273. DOI PubMed PMC
9. He J, Naik V, Horowitz LW. Hydroxyl radical (OH) response to meteorological forcing and implication for the methane budget. *Geophys Res Lett* 2021;48:e2021GL094140. DOI
10. Wang Y, Ming T, Li W, et al. Atmospheric removal of methane by enhancing the natural hydroxyl radical sink. *Greenh Gases* 2022;12:784-95. DOI
11. Wang Y, Zhang H, Zhang J, et al. Low-concentration methane removal: what can we learn from high-concentration methane conversion? *Catal Sci Technol* 2023;13:6392-408. DOI
12. Majdinasab A, Yuan Q. Performance of the biotic systems for reducing methane emissions from landfill sites: a review. *Ecol Eng* 2017;104:116-30. DOI

13. Smith P, Goulding KW, Smith KA, et al. Enhancing the carbon sink in European agricultural soils: including trace gas fluxes in estimates of carbon mitigation potential. *Nutr Cycl Agroecosys* 2001;60:237-52. DOI
14. Jackson RB, Abernethy S, Canadell JG, et al. Atmospheric methane removal: a research agenda. *Philos Trans A Math Phys Eng Sci* 2021;379:20200454. DOI PubMed PMC
15. Oeste FD, de Richter R, Ming T, Caillol S. Climate engineering by mimicking natural dust climate control: the iron salt aerosol method. *Earth Syst Dynam* 2017;8:1-54. DOI
16. Issaka E, Amu-Darko JN, Yakubu S, Fapohunda FO, Ali N, Bilal M. Advanced catalytic ozonation for degradation of pharmaceutical pollutants - a review. *Chemosphere* 2022;289:133208. DOI PubMed
17. Sun X, Li C, Yu B, Wang J, Wang W. Removal of gaseous volatile organic compounds via vacuum ultraviolet photodegradation: review and prospect. *J Environ Sci* 2023;125:427-42. DOI
18. Brodu N, Zaitan H, Manero MH, Pic JS. Removal of volatile organic compounds by heterogeneous ozonation on microporous synthetic alumina silicate. *Water Sci Technol* 2012;66:2020-6. DOI PubMed
19. Costa Filho BM, Vilar VJ. Strategies for the intensification of photocatalytic oxidation processes towards air streams decontamination: a review. *Chem Eng J* 2020;391:123531. DOI
20. Alejandro S, Valdés H, Manéro MH, Zaror CA. Oxidative regeneration of toluene-saturated natural zeolite by gaseous ozone: the influence of zeolite chemical surface characteristics. *J Hazard Mater* 2014;274:212-20. DOI PubMed
21. Reed C, Xi Y, Oyama S. Distinguishing between reaction intermediates and spectators: a kinetic study of acetone oxidation using ozone on a silica-supported manganese oxide catalyst. *J Catal* 2005;235:378-92. DOI
22. George C, Ammann M, D'Anna B, Donaldson DJ, Nizkorodov SA. Heterogeneous photochemistry in the atmosphere. *Chem Rev* 2015;115:4218-58. DOI PubMed PMC
23. Zhang J, Wang Y, Wang Y, et al. Solar driven gas phase advanced oxidation processes for methane removal - challenges and perspectives. *Chemistry* 2022;28:e202201984. DOI PubMed PMC
24. Chen W, He H, Liang J, et al. A comprehensive review on metal based active sites and their interaction with O_3 during heterogeneous catalytic ozonation process: types, regulation and authentication. *J Hazard Mater* 2023;443:130302. DOI PubMed
25. Zaitan H, Manero MH, Valdés H. Application of high silica zeolite ZSM-5 in a hybrid treatment process based on sequential adsorption and ozonation for VOCs elimination. *J Environ Sci* 2016;41:59-68. DOI
26. Zhao W, Zhang S, Ding J, Deng Z, Guo L, Zhong Q. Enhanced catalytic ozonation for NOx removal with $CuFe_2O_4$ nanoparticles and mechanism analysis. *J Mol Catal A Chem* 2016;424:153-61. DOI
27. Xiao J, Rabeah J, Yang J, Xie Y, Cao H, Brückner A. Fast electron transfer and $^{\bullet}OH$ formation: key features for high activity in visible-light-driven ozonation with C_3N_4 catalysts. *ACS Catal* 2017;7:6198-206. DOI
28. Peng J, Lu T, Ming H, et al. Enhanced photocatalytic ozonation of phenol by Ag/ZnO nanocomposites. *Catalysts* 2019;9:1006. DOI
29. Yang Y, Peng J, Tao H, et al. Synergistic effect of exposed facets and surface defects of ZnO nanomaterials for photocatalytic ozonation of organic pollutants. *Environ Sci Nano* 2023;10:1897-906. DOI
30. Li X, Ma J, He H. Recent advances in catalytic decomposition of ozone. *J Environ Sci* 2020;94:14-31. DOI
31. Corro G, Flores JA, Pacheco-Aguirre F, et al. Effect of the electronic state of Cu, Ag, and Au on diesel soot abatement: performance of Cu/ZnO, Ag/ZnO, and Au/ZnO catalysts. *ACS Omega* 2019;4:5795-804. DOI PubMed PMC
32. Du H, Li X, Cao Z, et al. Photocatalytic O_2 oxidation of CH_4 to CH_3OH on AuFe-ZnO bifunctional catalyst. *Appl Catal B Environ* 2023;324:122291. DOI
33. Jiang W, Low J, Mao K, et al. Pd-modified ZnO-Au enabling alkoxy intermediates formation and dehydrogenation for photocatalytic conversion of methane to ethylene. *J Am Chem Soc* 2021;143:269-78. DOI PubMed
34. Kavitha R, Kumar SG. A review on plasmonic Au-ZnO heterojunction photocatalysts: preparation, modifications and related charge carrier dynamics. *Mat Sci Semicon Proc* 2019;93:59-91. DOI
35. Luo L, Gong Z, Xu Y, et al. Binary Au-Cu reaction sites decorated ZnO for selective methane oxidation to C1 oxygenates with nearly 100% selectivity at room temperature. *J Am Chem Soc* 2022;144:740-50. DOI PubMed
36. Biglari H, Afsharnia M, Alipour V, Khosravi R, Sharafi K, Mahvi AH. A review and investigation of the effect of nanophotocatalytic ozonation process for phenolic compound removal from real effluent of pulp and paper industry. *Environ Sci Pollut Res Int* 2017;24:4105-16. DOI PubMed
37. Yao C, Chen W, Li L, et al. ZnO:Au nanocomposites with high photocatalytic activity prepared by liquid-phase pulsed laser ablation. *Opt Laser Technol* 2021;133:106533. DOI
38. Yang H, Li G, Jiang G, Zhang Z, Hao Z. Heterogeneous selective oxidation over supported metal catalysts: from nanoparticles to single atoms. *Appl Catal B Environ* 2023;325:122384. DOI
39. Jin R, Li G, Sharma S, Li Y, Du X. Toward Active-site tailoring in heterogeneous catalysis by atomically precise metal nanoclusters with crystallographic structures. *Chem Rev* 2021;121:567-648. DOI
40. Liu L, Corma A. Metal catalysts for heterogeneous catalysis: from single atoms to nanoclusters and nanoparticles. *Chem Rev* 2018;118:4981-5079. DOI PubMed PMC
41. Wang J, Liu D, Yuan S, et al. Understanding the plasmonic effect of enhanced photodegradation with Au nanoparticle decorated ZnO nanosheet arrays under visible light irradiation. *Molecules* 2023;28:6827. DOI PubMed PMC
42. Chen ZY, Shao WZ, Li WJ, Sun XY, Zhen L, Li Y. Suppressing the agglomeration of ZnO nanoparticles in air by doping with lower electronegativity metallic ions: implications for Ag/ZnO electrical contact composites. *ACS Appl Nano Mater* 2022;5:10809-17. DOI

43. Stefan M, Popa A, Toloman D, Leostean C, Barbu-Tudoran L, Falamas A. Enhanced plasmonic photocatalysis of Au-decorated ZnO nanocomposites. *Inorganics* 2023;11:157. DOI
44. Ma X, Li D, Jiang Y, et al. Fiber-like ZnO with highly dispersed Pt nanoparticles for enhanced photocatalytic CO_2 reduction. *J Colloid Interface Sci* 2022;628:768-76. DOI
45. Ren L, Li Y, Liu H, Zhao C, Zhao X, Xie H. Intensitive UV-Vis-IR driven catalytic activity of Pt supported on hierarchical ZnO porous nanosheets for benzene degradation via novel photothermocatalytic synergetic effect. *J Environ Chem Eng* 2022;10:107694. DOI
46. Phuruangrat A, Nunpradit A, Sakhon T, et al. Microwave-assisted synthesis of heterostructure Pd/ZnO flowers used for photocatalytic reaction of dyes illuminated by UV radiation. *J Aust Ceram Soc* 2021;57:1521-30. DOI
47. Zhou Q, Tan X, Wang X, et al. Selective photocatalytic oxidation of methane to methanol by constructing a rapid O_2 conversion pathway over Au–Pd/ZnO. *ACS Catal* 2024;14:955-64. DOI
48. Chen J, Zhu W, Zhao W, et al. Revelation of contributing mechanism of reactive oxygen species in photocatalytic ozonation heterocyclization of gaseous hexane isomers. *Chemosphere* 2023;316:137759. DOI